Available online at BCREC website: https://bcrec.id

Bulletin of Chemical Reaction Engineering & Catalysis, 18 (1) 2023, 1-16

Research Article

Photodegradation of Methylene Blue with Aid of Green Synthesis of CuO/TiO_2 Nanoparticles from Extract of *Citrus Aurantium* Juice

Shahnaz Bassim, Alyaa K. Mageed*, Adnan A. AbdulRazak, Farooq Al-Sheikh

Chemical Engineering Department, University of Technology, Baghdad, Iraq.

Received: 11th November 2022; Revised: 30th December 2022; Accepted: 31st December 2022
Available online: 13rd January 2023; Published regularly: March 2023

Abstract

Green synthesis methods using plants have many advantages such as time-saving, chemical-free, and negative effects on the environment. So, extracted *Citrus aurantium* juice was used to synthesize green CuO/TiO_2 and (G-CuO/TiO_2) nanocatalyst which was characterized by X-ray Diffraction (XRD), Scanning Electron Microscopy (SEM), Energy Dispersive X-ray (EDX), Fourier Transform Infra Red (FTIR), Brunauer-Emmett-Teller (BET), and Zeta Potential (ZP), and utilized in the degradation of methylene blue (MB) under UV lamps and dark environments. The ANOVA program was used to maximize the photodegradation efficiency (%) of (G-CuO/TiO_2) on the MB dye. The four independent variables: Initial dye concentration (10-50 mg/L), pH (3-9), adsorbent dose (200-1000 mg/L), and contact time (30-90 min) served to the model of the photodegradation efficiency (%). The ANOVA results confirmed the high significance of the regression model while the predicted values of the photodegradation efficiency (%) of MB were in good agreement with the corresponding experimental ones. Optimized conditions for the maximum photodegradation efficiency (98.6%) by (G-CuO/TiO_2) NPs were the initial dye concentration (10.93 mg/L), pH (8.87), adsorbent mass (986.43 mg/L), and contact time (89.08 min). The validity of the quadratic model was examined, and found in good agreement with the experimental values. Results demonstrated that (G-CuO/TiO_2) could be a promising photocatalyst in the degradation of MB dye.

Keywords: Photocatalytic Degradation; Nanoparticle Cuo-TiO_2; Citrus aurantium juice; Methylene Blue

How to Cite: S. Bassim, A.K. Mageed, A.A. AbdulRazak, F. Al-Sheikh, (2023). Photodegradation of Methylene Blue with Aid of Green Synthesis of CuO/TiO_2 Nanoparticles from Extract of *Citrus Aurantium* Juice. *Bulletin of Chemical Reaction Engineering & Catalysis*, 18(1), 1-16 (doi: 10.9767/bcrec.16417)

Permalink/DOI: https://doi.org/10.9767/bcrec.16417

1. Introduction

Paper and food industries, textile dyeing, cosmetics, pigments and paints, high technology materials, etc. employ organic and inorganic colorants extensively [1]. On the other hand, most organic dyes utilized by many sectors nowadays are synthetic. Oil-based intermediates are frequently used to create organic colors. Meanwhile, industrial processes use more than 100,000 different kinds of synthetic organic colorants. Industrial effluents may contain about 10-15% of these colors [2]. Dyes are one of these dangerous organic pollutants that are predominantly emitted into the environment by the textile and painting industries [3]. These colors produce deadly carcinogenic byproducts when they hydrolyze and combine with other contaminants found in wastewater effluents, endangering not only human health and well-being but also the aquatic ecosystem [4]. Wool and silk are frequently dyed with the basic dye methylene

* Corresponding Author.
Email: alyaa.k.mageed@uotechnology.edu.iq (A.K. Mageed);

blue (MB) [5,6]. It is also employed in medicine to check for certain disorders. Many treatment methods have been developed recently to remediate these wastes [7].

Environmentally benign and economical, the adsorption technique is preferred. It has a high yield of purification, and the choice of adsorbent is crucial in deciding how cost-effective it is. Without effective degradation, substances found in bodies of water including rivers, lakes, and seas have negative side effects like eye burns, diarrhea, vomiting, and nausea [8]. Finding an effective way to clean wastewater that contains dyes has thus become a key research objective. The degradation of organic contaminants in contaminated wastewater is thought to be made possible by photocatalysis, a green technology [9]. Metal oxide nanoparticles have a wide range of noteworthy applications, including cell line research, antimicrobial, and dye degradation [10]. Titanium is a widely used-wide band gap semiconductor that has long been the preferred material for photocatalysis. However, due to its relatively broadband gap (3-3.2 eV) and high rate of electron-hole recombination, it has several drawbacks [11]. Therefore, significant efforts have been made to modify titanium-based photocatalysts to allow for the use of solar radiation visible spectrum [12]. The main issue in this sector is to develop a photocatalyst material that is effective, affordable, and sustainable that can operate in the presence of visible light. TiO_2 exhibits the highest rate of photocatalytic activity for the correct removal and total elimination of organic contaminants among other semiconductors. TiO_2 is a promising contender for photocatalytic and antibacterial activity because of its better chemical stability, photostability, environment friendliness, strong oxidizing power, cost-effectiveness, and non-toxicity [13]. G-CuO/TiO_2 is believed to be easily synthesized and may have been used in photocatalytic dye hydrolysis and antibacterial action against pathogenic microorganisms [14].

The researches in this field are many: Rajiv *et al.* [15] used *Momordica charantia* leaf aqueous extract as a reducing and stabilizing agent to biosynthesize TiO_2 nanoparticles (NPs) used in the in vitro antimalarial activity against Plasmodium falciparum, and the findings imply that the produced TiO_2 NPs may be used to create novel, safer malaria prevention treatments. In a related study, Goutam et al [16] prepared green titanium dioxide NPS using leaf extract of the biodiesel plant, *Jatropha curcas L.*, and assessed its performance for the photocatalytic treatment of TWW following the secondary (biological) treatment process, achieving 82.26 and 76.48 percent of COD and Cr removal, respectively, in a parabolic trough reactor (PTR). Additionally, *Padina tetrastromatica* extract was used by Jegadeeswaran *et al.* [17] to create innovative, environmentally friendly Ag/TiO_2 nanocomposites with an anatase phase and an average particle size of 25.74 nm. Plants contain chemical compounds that can now be used for a variety of applications, including water purification, medicinal, and other uses.

Accordingly, the present work focuses on 1) studying the synthesis and structural characterization of CuO/TiO_2 nanoparticles from green synthesis on citrus aurantium juice using FTIR, SEM, EDX, XRD, and the surface area and pore size on the adsorbent surface (BET), 2) determining the effect of the introduction of doping elements on the chemical and structural properties, 3) The nanostructured TiO_2 was synthesized of 2:1 CuO of the co-sedimentation method, and 4) obtained G-CuO/TiO_2 was used in the degradation of methylene blue under UV lamps and a dark environment.

2. Materials and Methods

2.1. Materials

Citrus aurantium juice extract was obtained from the local market in Baghdad, Iraq. The materials used in the experiments included oxide Titanium (TiO_2), Cupric sulfate Pentahydrate ($CuSO_4.5H_2O$), Sodium hydroxide (NaOH), Sodium chloride (NaCl), hydrochloride acid (HCl), and Methylene blue ($C_{16}H_{18}CIN_3S.XH_2O$). All chemicals and reagents were analytically graded and purchased from HiMedia (Thane, India).

2.1.1 Preparation of *Citrus aurantium* juice

To prepare the extract of *Citrus aurantium*, 5 kg of *Citrus aurantium* was thoroughly washed with distilled water to remove any dust, after which it was cut and squeezed to extract the juice. Then it was heated for 30 min at 80 °C. After being cooled to room temperature, the filter paper was used to remove the remaining sediment. Later, it was stored as pure extract without the filler for more experimental work as in Figure 1.

2.1.2 Synthesis of (G-CuO/TiO_2) NPs

In the synthesized (G-CuO/TiO_2) NPs, 0.79 g of titanium oxide (TiO_2) and 1.6 g of $CuSO_4.7H_2O$, were mixed with 100 mL distilled

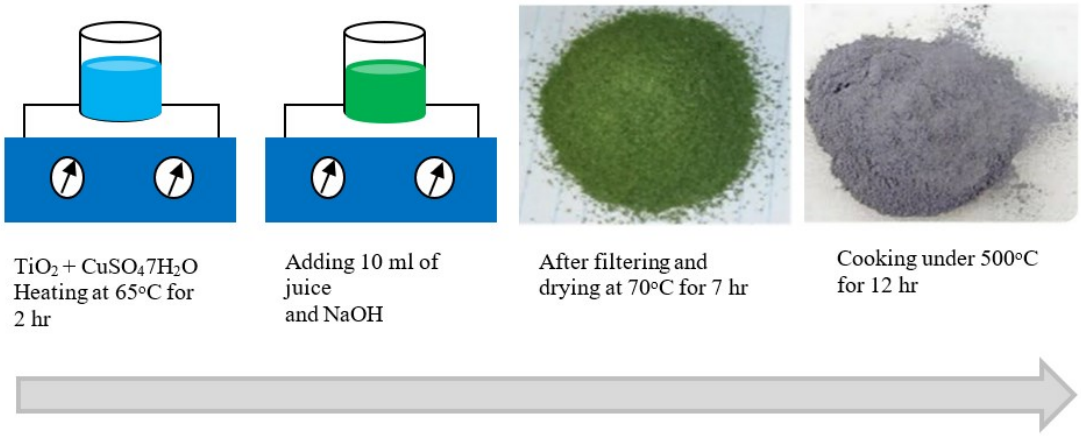

Figure 1. Preparation of (G-CuO/TiO_2).

Table 1. High, center, and low levels of the independent variables investigated in the present study.

Variables	Levels and range		
	(+1)	(0)	(+1)
Initial dye concentration (A) (mg/L)	10	30	50
Solution pH (B)	3	6	9
Adsorbent dose (C) (mg/L)	200	600	1000
Contact time (D) (min)	30	60	90

Table 2. Experimental design data in relation to photodegradation efficiency (%).

Run no.	A: Initial con., mg/L	B: pH	C: Adsorbent dose, mg/L	D: Time, min	Photodegradation efficiency, %
1	30	6	600	90	65.20
2	30	9	600	60	82.50
3	30	6	600	60	62.89
4	50	3	1000	30	52.67
5	10	3	200	90	30.67
6	50	3	1000	90	75.00
7	30	6	200	60	49.45
8	30	6	600	60	62.89
9	50	9	1000	90	88.45
10	30	6	600	30	55.39
11	10	9	200	30	86.23
12	30	6	600	60	62.89
13	10	9	1000	30	85.76
14	50	6	600	60	59.29
15	30	6	600	60	62.89
16	30	6	600	60	62.89
17	50	9	200	30	64.78
18	10	3	1000	90	70.12
19	30	6	600	60	62.89
20	30	3	600	60	42.67
21	50	9	1000	30	66.34
22	10	3	1000	30	55.70
23	10	9	1000	90	97.50
24	10	6	600	60	70.50
25	30	6	1000	60	75.53
26	10	3	200	30	22.78
27	50	3	200	90	41.54
28	50	9	200	90	68.45
29	50	3	200	30	24.88
30	10	9	200	90	92.30

water at 65°C for 5 h, and 10 mL of the juice extract was added under continuous mixing for 30 min. Then, drops of 0.1 N sodium hydroxide were added to the mixture, and mixing continued for 1 h at 80 °C until the color of the solution changed from light blue to green. Then, the solution was filtered with (0.55 nm) filter paper, after which it was washed several times with deionized water and ethanol, and next dried in an oven for 12 h at 70 °C, finally, the calcination of the synthesized (G-CuO/TiO_2) NPs was done in the thermal oven at 500 °C for 2 h [18].

2.1.3 Characterization

Energy-dispersive X-ray spectroscopy analysis (EDX), scanning electron microscopy (SEM), X-ray diffraction (XRD), and Brunauer–Emmett–Teller (BET) measurements were used to characterize the TiO_2-CuO NPs samples. EDX and SEM analyses were conducted using a Bruker INSPECT550 (Leiderdorp, Netherlands). The XRD measurements were conducted by Shimadzu-6000 (Kyoto, Japan) at the Cu-Kα wavelength (λ = 0.1524 nm) with 2θ ranging from 5 to 80°. In addition, the Brunauer–Emmett–Teller (BET) method was conducted using the surface area analyzer (Q-surf 9600, USA).

2.2 Experimental Design

In this work, Design-Expert 7.0.0 software (Stat-Ease Inc., USA) was used, where the central composite design (CCD) using a response surface methodology (RSM) was applied to correlate and optimize four operation process variables (*i.e.*, initial dye concentration; solution pH; adsorbent dose; and contact time) about the Photodegradation efficiency (%) of the MB dye. The minimum and maximum ranges of the variables were as follows: Initial dye concentration (*A*) (10-50 mg/L), solution pH (*B*) (3-9), adsorbent dose (*C*) (200-1000 mg/L), and contact time (*D*) (30-90 min). Table 1 presents the high, center, and low levels of the four independent variables investigated while Table 2 represents the experimental data in this study.

2.3 Photodegradation Studies

TiO_2 is known to use a UV bandwidth to initiate a photoreaction at 3.2 eV. Copper oxides display an improved absorber with a narrow band gap (1.4-2.2 eV). Copper oxides with TiO_2 are mentioned to give greater catalytic ability and greater photocatalytic efficacy. Several investigations have investigated the detection of toxic substances from industrial activities (e.g., xylene, dyes, phenol, and pesticides) through the use of homogeneous photocatalytic processes using constant UV radiation [19,20]. With respect to the presence of compatible functional groups, the *Cytrus aurantium* juice was reported to contain 86% of phenolic acids out of total phenolic compounds. The phenolic compounds present in the citrus aurantium juice such as (Gallic, Sinapic, Dihydroxyphenilic, Dihydrobenzoic, Chlorogenic, Vanillic, Syringic, *p*-coumaric, Ferulic, Rosmarinic, trans-2-Dihydrocinnamic, and cinnamic acids). The surface electrons on the CuO nanoparticles should finally transfer to the dye in the dark when the CuO-TiO_2 nanocatalysts are disseminated in the solution with an organic pollutant. However, electrons (e^-) in the valence band (VB) can be excited to the conduction band with the simultaneous creation of the equivalent quantity of holes (h) in the valence band when these catalysts are exposed to UV light with photon energy higher or equal to the band gap of TiO_2. Reactions are hypothesized to be in charge of the dye degradation when CuO-TiO_2 nano photocatalyst is used.

$$\text{CuO-TiO}_2\ (e^-_{CB}) + \text{CuO-CB\_} + \text{CuO-TiO}_2\ (h^+_{VB}) \quad (1)$$

$$\text{CuO-TiO}_2\ (e^-_{CB}) + \text{Dye} \rightarrow \text{Products} \quad (2)$$

$$\text{CuO-TiO}_2\ (h^+_{VB}) + \text{Dye} \rightarrow \text{Photo bleached Products} \quad (3)$$

When CuO-TiO_2 surfaces are exposed to light photons with an energy larger than 3.2 eV, electron-hole pairs (e^-, h^+) are created. When these pairs are joined with H_2O molecules and dissolved oxygen, hydroxyl radicals (OH) are produced. In addition, (H^+) ions, superoxide (O_2^+), and peroxide (OOH) radicals are produced. H and (*OOH) combine to form OH and OH^-. The (h^+) converts OH^- to OH. As a result, all species increase the production of OH. The many poisonous chains that are present in the liquid are broken up by these radicals [21].

The photodegradation MB was conducted randomly by employing batch experiments in an aqueous solution using (G-CuO-TiO_2) as a catalyst. All experiments were carried out in a shaker (KS10, Edmund Buhler, Germany) at 300 rpm, where 200 mL conical flasks were filled with 50 mL of the MB solution of a known initial concentration (10-50 mg/L), and a specific mass of (G-CuO-TiO_2) (200-1000 mg/L) was added at a controlled pH level (3-9). The pH of the solution was measured using a pH 9124 electronic device made by HANNA

(Rhode Island, USA). The solution was allowed to equilibrate in darkness, and when the equilibrium was attained, the mixture was radiated under the UV lamp (100 W) for a contact time of 30-120 min. The solution was filtered using a centrifuge at 10000 rpm for 15 min. A UV-visible spectrophotometer (λ_{max}-664 nm) was used to calculate the dye concentration and the ratio of the % removal as follows:

$$Photodegradation\ efficiency(\%) = \frac{C_i - C_0}{C_0} \times 100 \quad (4)$$

where, C_i and C_0 are the initial and final MB concentrations, respectively.

For engineering purposes, it is useful to find out a simple and easy-to-use rate equation that fits the experimental rate data. Finding the reaction kinetics and determining rate laws are necessary to enable the large-scale use of photolysis techniques. The work of MB photocatalytic degradation kinetics can be explained as follows [22]:

$$\ln\left(\frac{C_0}{C_t}\right) = -K_1 t \quad (5)$$

where, C_0, and C_t are MB concentrations (g/L) at initial and time (t) respectively, K_1 (min) is the rate constant of the pseudo-first-order equation, and t is the time.

3. Results and Discussion

3.1 Characterization of the (G-CuO/TiO$_2$) Nanoparticles

Figure 2 shows the XRD of CuO/TiO$_2$. The results for the CuO/TiO$_2$ sample confirm the presence of CuO crystallites (JCPDS 41–0254) [23] and TiO$_2$ in the anatase phase (JCPDS 21–1272) [24]. Two peaks at 2θ = 35.8° and 38.4° in the XRD pattern correspond to CuO, which are the (002) and (101) planes, respectively. The strength of these characteristic peaks was

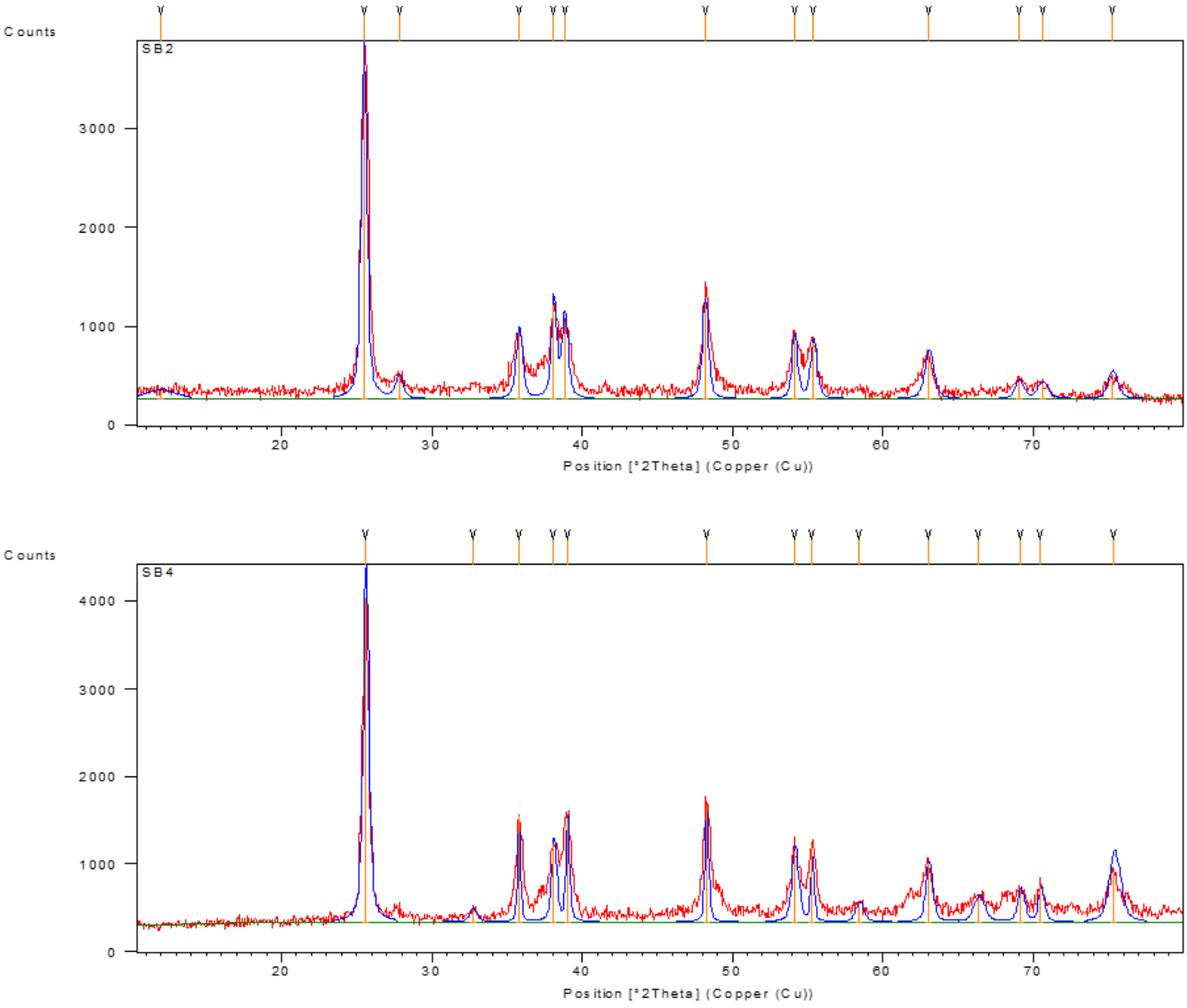

Figure 2. XRD plot of CuO/TiO$_2$ and G-CuO/TiO$_2$.

significantly enhanced with the increase of added $CuSO_4.5H_2O$ Also, the sharp, intense peak at 2θ = 25.281° corresponds to the anatase (101) phase, representing that the synthesized nanomaterials were well crystallized. The crystallite sizes of (G-CuO/TiO_2) were estimated by Scherrer's equation [25], using the most intense reflection (2θ = 25.2818°). The particle sizes of the sample were computed at 10.46 nm.

Surface features (*i.e.*, specific surface area and pore volume) are crucial elements that must be studied because they have a significant impact on the photocatalytic activity. Table 3 provides the BET surface area and pore volume of the CuO/TiO_2, and (G-CuO/TiO_2). The tabulated results show that the surface area and pore volume of (G-CuO/TiO_2) were greater than those of (CuO/TiO_2), this is due to the carbonization of the (G-CuO/TiO_2) at 550 °C.

SEM was used to study the morphological properties of copper (TiO_2-CuO). The particles were discovered to be clumped together. According to earlier research, metal oxidation is the sole process that may cause such agglomerations. It puts up a roadblock in the way of research on specific NPS structures, in the illustration, the bulge, and rough surface in Figure 3(a). On the other hand, the SEM picture in Figure 3(b) for TiO_2-CuO/CA after doping (CA) is taken after the particles had been calcined at 550 °C. In comparison to TiO_2-CuO, large agglomerates of various sizes and shapes can be seen in the microscope in Figure 3(a). The formation of the big agglomerates resulted from the calcination process, which reduced the aurantium juice's structure to minute particles with a vast surface area [26]. Where the microscopic image associated with calcination at 550 °C and the loss of small pore size is depicted in Figure 3(b). It might be caused by the pores collapsing, as evidenced by the presence of a sizable hole on the surface. The size of the nanoparticles was estimated from the particle size distribution analysis that was carried out using SEM at about 68.59 nm and the surface shape of TiO_2 was visualized before loading. With particle size analysis and after loading, the diameters were from 26 nm to 49.62 nm, where large agglomerations were noted [27]. This demonstrates that the surface rate can alter the size and form of particles in addition to affecting how they disperse. The particle size of the modified sample is less than 60 nm, according to the SEM analysis of TiO_2-CuO. The surface morphological perfectly illustrates the doping (CA) on the TiO_2-CuO material's surface. With its porous nature, it demonstrates that the particle structures are irregular and caused a minor rise in surface area to 55.184, which is ascribed to the juice's surface porosity.

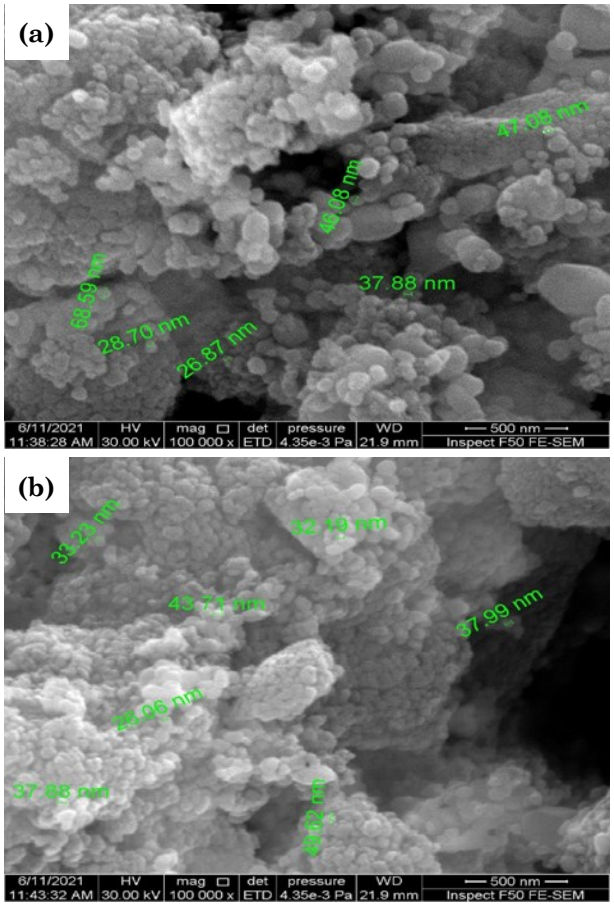

Figure 3. SEM of (a) CuO/TiO_2, and (b) (G-CuO/TiO_2).

An EDX analysis was performed for the samples as shown in Figure 4. Peaks of the TiO_2-Cuo graph were (C: 10.1, N: 0.7, O: 29.4, AL: 0.3, Ti: 26.1, Cu: 33.4), and the TiO_2-Cuo/CA nanoparticles were (C:18.6, N: 5.1, O: 36.5, AL: 0.3, Si:0., Ca:0.5, Ti: 16.5, Fe: 0.3, Co: 0.1, Ni: 0.3, Cu: 21.5), The decrease in O, Ti, Cu is due to an increase in temperatures to 550°C, which is due to the formation of TiO_2-CuO/CA, as well as an increase in new peaks of the TiO_2-CuO nanocomposite, which confirms that citrus aurantium juice possesses effective functional groups and an MB.

Table 3. Textures attributes of Cu-TiO_2 and (G-CuO/TiO_2).

Properties	CuO/TiO_2	(G-CuO/TiO_2)
S_{BET}, m^2/g	25.941	55.184
V_M, cm^3/g	6.1898	12.4452

For the CuO-doped TiO_2 spectrum the O–H group is shown at the peaks of 3460 and 1722 cm^{-1} [28]. Vibrations of Ti–O and Ti–O–Ti framework bands of TiO_2 can be attributable to the peaks of TiO_2, at 476, and 620 cm^{-1} [29]. It represents a band at 459 cm^{-1}. Also, the wide vibrational band (between 400 and 600 cm^{-1}) could be assigned as a metal-oxygen (Cu–O and Ti–O) stretching vibration [30]. The FTIR of (CuO-TiO_2) after loading citrus aurantium juice was shown in Figure 5. The large absorption peak of titanium and copper nanoparticles was observed at 3441.1 cm^{-1}. The presence of ammonium ions with the expansion of N–H and the average peak at 1581.63 cm^{-1}. The compound is shown to shave with C–C expansion after adding juice was reflected by the presence of a higher concentration of obtaining phenols with the extension of O–H and the peak at 2970.38 cm^{-1}. Then represent the aromatic ethers of the C–O extension by the peak at 1288.45 cm^{-1}. Peaks observed at 1122.57 cm^{-1} are shown for alcohol compounds with the C–O expansion. Aliphatic insurances are shown with a C–N extension at the peak of 1060.85 cm^{-1}. Peaks 964.41 and 918.12 cm^{-1} confirm the presence of a strong double-alkene double bond, and the other section at 779.24 cm^{-1} and 636.51 cm^{-1} confirm the presence of a C–Br, C–Cl bond. Previously, similar peaks for TiO_2-CuO NPs synthesized using Calotropis gigantean extract were also reported by [31]. After juice addition, the most recent iteration of the Citrus aurantium juice (CA) match with the CuO-TiO_2 Nano composite demonstrated a match with functional groups that were previously reported by previous researchers [32]. In Figure 5, after photodegradation of the dye, different peaks were found 3421.72, 2974.24, 1573.91, 1423.47, 1107.14, 821.68, 964.41, 686.66,

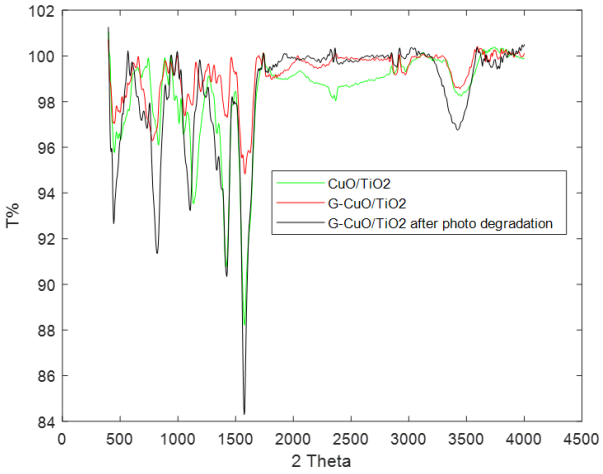

Figure 5. FTIR of CuO/TiO_2, $G\text{-}CuO/TiO_2$, and $G\text{-}CuO/TiO_2$ after photodegradation.

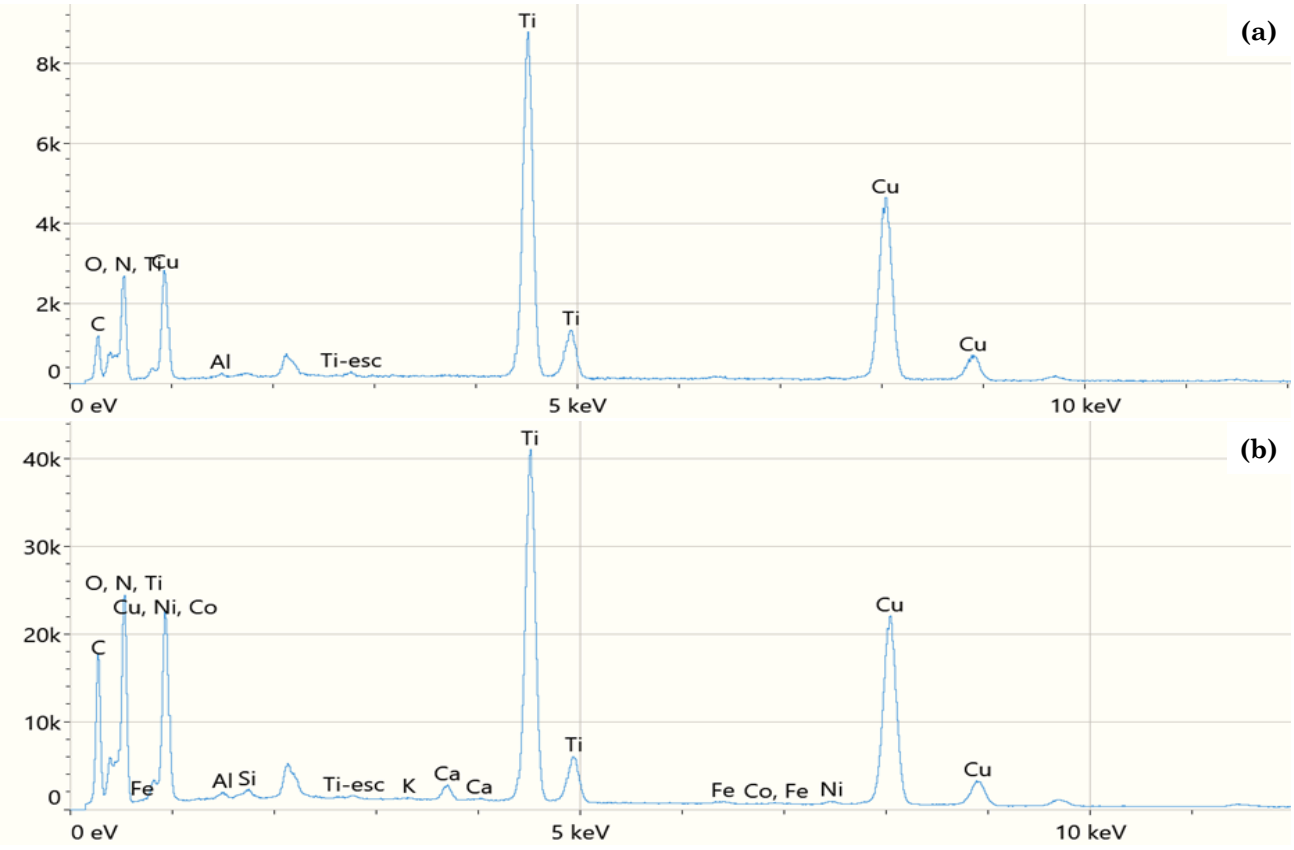

Figure 4. EDX of (a) CuO/TiO_2 and (b) $G\text{-}CuO/TiO_2$.

586.36, and 443.63 cm^{-1}, this confirms that the peaks remained preserving the functional groups associated with the stretching oscillations N−H, C−N, C−C, C−H, C−O, polyols respectively. And peaks less than 3000 cm^{-1} are due to C−H stretching and C−N stretching.

3.2 Experiment Studies

The (G-CuO/TiO_2) nanoparticles were used in the experiment to evaluate the photocatalysis of methylene blue dye on the surface of (G-CuO/TiO_2) using UV.VIS light. For this investigation, a constant temperature of 25 °C was used along with catalyst loading of 200-1000 mg/L, a pH range of 3–9, and an initial dye concentration of 10–50 mg/L at various times. A spectrophotometer (UV-VIS) operating at a wavelength of 664 nm was used to measure the residual amount of methylene blue.

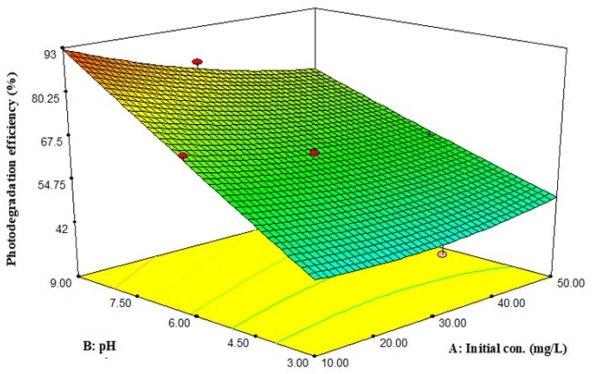

Figure 6. Interaction effect between initial dye concentration and the solution pH on the photodegradation efficiency (100%) at a constant contact time of 60 min and adsorbent dose 600 mg/L.

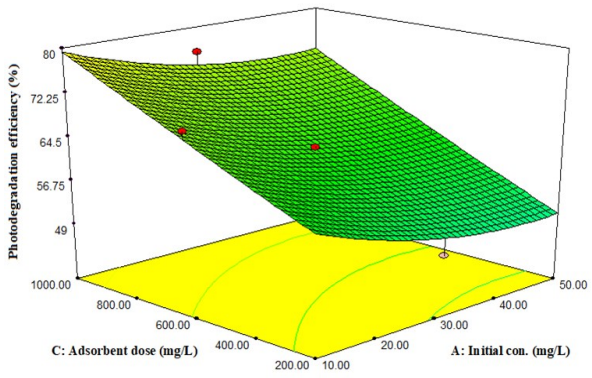

Figure 7. Interaction effect between initial dye concentration and the Adsorbent dose on the % photodegradation efficiency at a constant contact time of 60 min and pH = 6.

3.2.1 Combined effect of variables on MB dye removal

Design-Expert 7.0.0 software was used to evaluate the influence of each operation variable and their Interaction on the photodegradation efficiency (%), as shown in Figures 6-11.

3.2.2 Effect of pH and initial dye concentration

Figure 6 examines the combined effect of the initial concentration of the dye and the pH solution on the photodegradation efficiency of (G-CuO/TiO_2) on MB at constant a constant contact time of 60 min and adsorbent dose of 600 (mg/L). The pH of the methyl orange solution was adjusted with HCl and NaOH. Across the entire initial concentration of the dye range (10-50) mg/L, it can be seen from Figure 6 that the pH of the solution has a great influence on the photocatalytic degradation, when the pH = 3, the photodegradation efficiency was 46.37%, when the pH = 9, the photodegradation efficiency increased to 92.6%. The relationship between pH and photocatalytic degradation can be described as the pH_{ZPC} of the (G-CuO/TiO_2) pH_{ZPC} = 7.6). Since MB is a catatonic dye, when the reaction system is alkaline, the enriched OH in the system makes the catalyst surface a negative charge, which is more conductive to the adsorption of dye molecules [33]. On the other hand, when the reaction system is acidic, the enriched H, in the system inhibits the adsorption of the dye molecules by the catalyst. The initial concentration has less influence on the photocatalytic degradation, under the conditions of the same pH = 9, an increase in the initial concentration from 10 to 50 mg/L caused a decrease in photocatalytic degradation of the MB dye from 92.6% to 73.72%. This is due to a

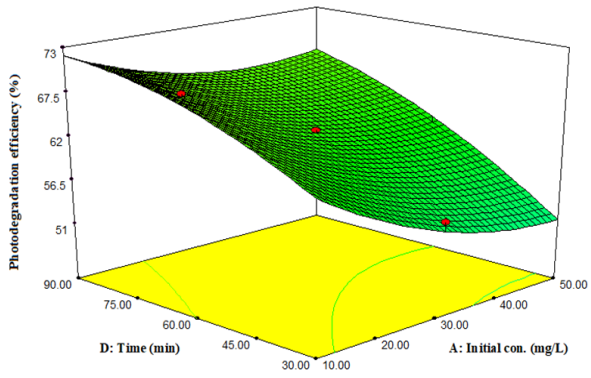

Figure 8. Interaction effect between initial dye concentration and the contact time on photodegradation efficiency (%) at a constant Adsorbent dose of 600 mg/L and pH = 6.

high concentration of dye, the solution becomes more intense colored and the path length of photons entering the solution decreased [34].

3.2.3 Effect of adsorbent dose and initial dye concentration

Figure 7 represents the effect of initial dye concentration and adsorbent dosage at a fixed pH of 6 and contact time of 60 minutes. It clearly shows that the adsorbent dosage had positive effects on the photodegradation efficiency, whereas the photodegradation efficiency increased with increases in the adsorbent dosage across the entire initial dye concentration 10-50 mg/L. This may be as the catalyst amount increases the active sites on the surface of the catalyst increase, which in turn enhances the photoreaction [35].

3.2.4 Effect of contact time and initial dye concentration

Figure 8 shows the interactive effect of the initial dye concentration and contact time at a constant adsorbent dose of 600 mg/L and solution pH of 6 on photodegradation efficiency (%). The photodegradation efficiency (%) increased as the MB dye concentration decreased. The percentage of MB degradation is directly related to the contact time, which means degradation increases with increasing contact time [36], this may be explained based on increasing time more and more light energy falls on the catalyst surfaces which induced the formation of photon excited species and enhances the photocatalytic activities [37].

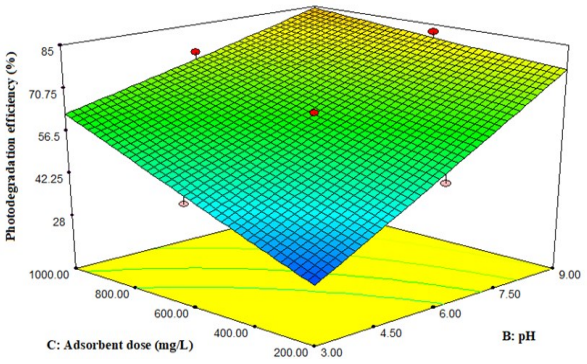

Figure 9. Interaction effect between adsorbent dose and the pH on the photodegradation efficiency (%) at a constant initial dye concentration 30 mg/L and contact time 60 min.

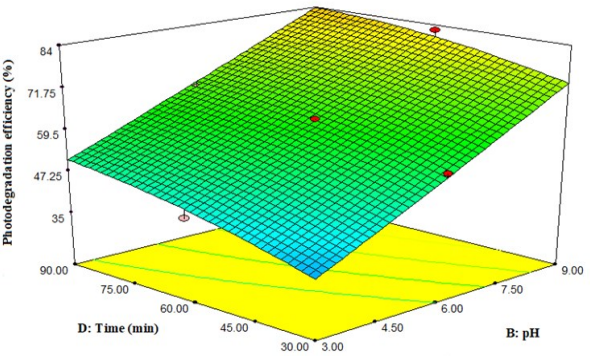

Figure 10. Interaction effect between contact time and the pH on the photodegradation efficiency (%) at a constant initial dye concentration of 30 mg/L and Adsorbent dose of 600 mg/L.

3.2.5 Effect of pH and adsorbent dose

Figure 9 depicts the interaction between the catalyst dose and pH of the solution at a constant time of 60 min and a starting dye concentration of 30 mg/L. It clearly shows that the adsorbent dosage had positive effects on the photodegradation efficiency (%), whereas the photodegradation efficiency (%) increased with increases in the adsorbent dosage across the entire pH range (3-9) of the solution. As can be seen in Figure 9, the lines are not elliptical, which indicates that there is no interaction between the adsorbent dose and the pH.

3.2.6 Effect of pH and contact time

The response surface plot for the effect of the pH and contact time on the photodegradation efficiency (%) at a constant initial dye concentration of 30 mg/L and adsorbent dose of 600 mg/L is shown in Figure 10. Time had a noticeable effect on the photodegradation efficiency (%). The photodegradation of MB initially increases gradually by increasing the contact time and then becomes constant after a particular time [38]. This is due to the availability of a large number of active sites, the degradation rate is faster for the first 75 min, and then it

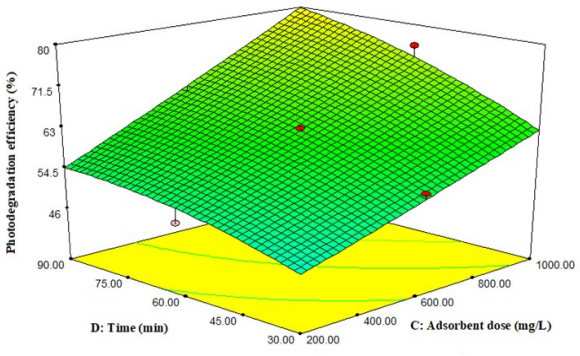

Figure 11. Interaction effect between contact time and the Adsorbent dose on the photodegradation efficiency (%) at a constant initial dye concentration of 30 mg/L and pH= 6.

attains equilibrium. It means that after these 75 min there will be repulsion between dye particles and the catalyst surface which lowers the degradation rate [36].

3.2.7 Effect of adsorbent dose and contact time

Figure 11 represents the effect of the adsorbent dose and contact time at a fixed initial dye concentration of 30 mg/L and pH 6. It clearly shows that the contact time had positive effects on the photodegradation efficiency (%), whereas the photodegradation efficiency (%) increased with increases in the contact time across the entire adsorbent dose range 200-1000 mg/L.

3.2.8 Point of zero charge pH_{pzc}

Figure 12 shows the zeta potential of (G-CuO/TiO_2) at varying pH levels. The positive values of the (G-CuO/TiO_2) zeta potential changed to negative values = 7.6 (pH_{pzc}). At a pH of 9, the negatively charged surface of the adsorbent most significantly affected the adsorption of the MB dyes due to the electrostatic attraction between the negative surface charge and the cationic dye [39]. In contrast, at pH of 3, the protons competed with the MB dyes in trying to adsorb onto the available surfaces; as a result, the percentage of dye removal decreased under these acidic conditions.

3.2.9 Recycle photodegradation

The cyclic photodegradation performance of (G-CuO/TiO_2) was studied in this work. Upon completion of the MB photodegradation, the (G-CuO/TiO_2) particles were separated from the reaction mixture, washed with distilled water, and reused for the photodegradation of MB dye. As shown in Figure 13, the photodegradation efficiency (%) of (G-CuO/TiO_2) after five rounds of cyclic photodegradation accounted for 97.5, 96.7, 94.8, 93.39, and 91.67 % at the following conditions: pH = 9, adsorbent dose = 1000 mg/L, initial concentration = 10 mg/L, and time = 90 min. Thus, the evidence indicates that (G-CuO/TiO_2) is stable and reusable in photodegradation of the MB dye from wastewater.

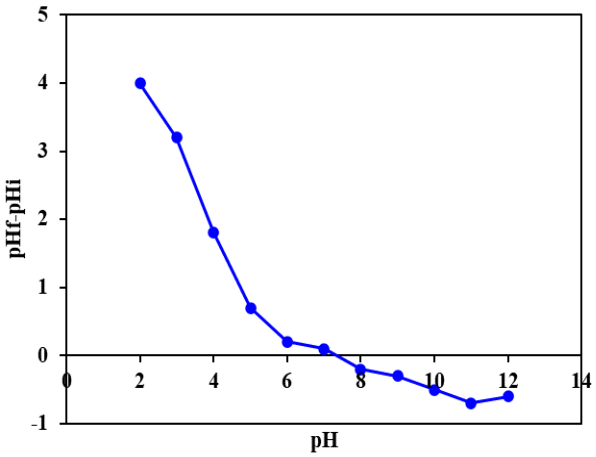

Figure 12. Zero potential charge (G-CuO/TiO_2).

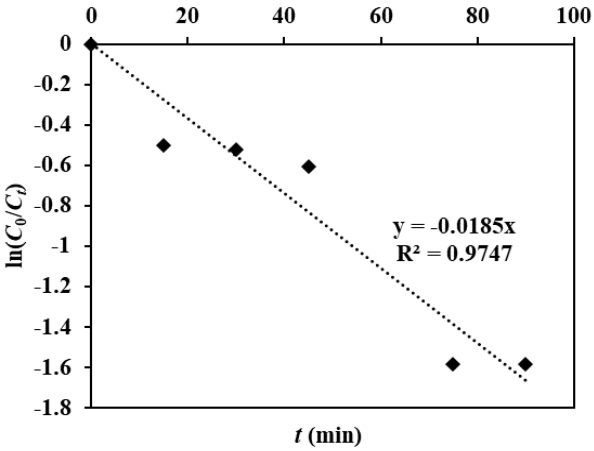

Figure 14. First-order equation at 10 ppm.

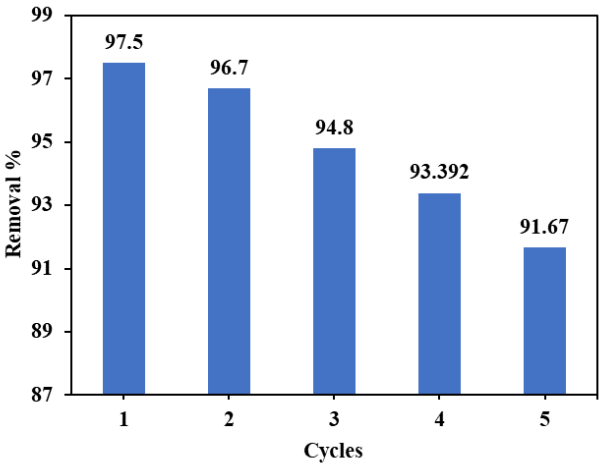

Figure 13. Recycling CuO-TiO_2/CA.

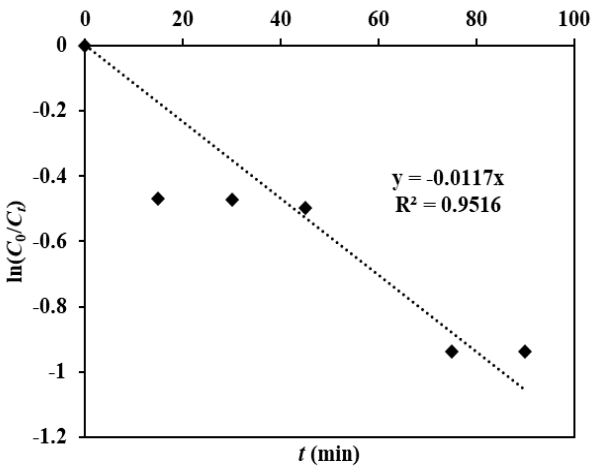

Figure 15. First-order equation at 50 ppm.

3.3 Photodegradation Kinetics

Figures 14 and 15 show the linear relation between ln (C_0/C_t) versus t at 10 and 50 mg/L respectively to represent the pseudo-first-order kinetic model at 1000 mg/L, and pH 9. The results show that the constant rates were 0.018 and 0.011 with R^2 values were 0.92 and 0.80 for 10 and 50 mg/L, respectively. These results demonstrate that the photocatalytic decomposition of MB dye in aqueous solutions using (G-CuO/TiO_2) nanoparticles can be described by a pseudo-first-order kinetic model. A similar study of MB adsorption was performed on TiO_2 nanoparticles as photocatalyst [40].

3.4. Experimental Design and Quadratic Model

The experimental results of the photodegradation efficiency (%) were modeled using RSM combined with a backward regression method, which was performed automatically in Design-Expert 7.0.0. The developed model for photodegradation efficiency (%) used a second-order polynomial quadratic equation in terms of the coded factors, as follows:

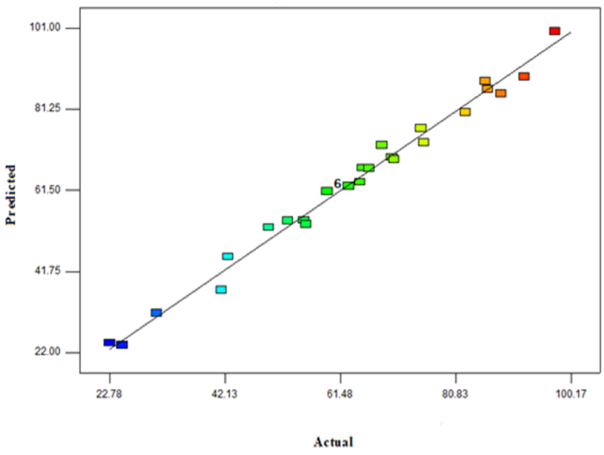

Figure 16. The predicted versus the actual photodegradation efficiency (%) of MB by (G-CuO/TiO_2).

$$\begin{aligned} \textit{Photodegradation efficiency}\ (\%) = 62.56 \\ -3.90A+17.57B+10.33C+6.37D \\ -5.54AB+1.54AD-6.71BC \\ +2.27CD \end{aligned} \quad (6)$$

where, A pertains to the initial dye concentration, B denotes the solution pH, C is the amount of catalyst and D is the contact time. In the above model, positive signs point to these variables exerting a positive effect on the photodegradation efficiency (%), whereas negative signs point to an antagonistic effect on the photodegradation efficiency (%). The positive value relating to the solution pH (B), the amount of catalyst (C), and (D) contact time had a positive effect, as these terms increased the photodegradation efficiency (%). Conversely, the negative value relating to the initial concentration (A) indicates that it exerted an antagonistic effect on the photodegradation efficiency (%). To study the adequacy and significance of the current model, an ANOVA test was performed, with the results presented in Table 4. The p-value was set at <0.05, and the F-value was high, at 9867.64. These results indicate that the second-order quadratic model was adequate for describing the MB photodegradation process using (G-CuO/TiO_2). Values of "Prob > F" less than 0.05 indicate that the model terms are significant. In this case, A, B, C, D, AB, and BC are significant model terms. The accuracy of the above model was evaluated in terms of the regression coefficients (R^2), adjusted R^2, and predicted R^2, which were 0.9875, 0.9759, and 0.9110, respectively. The actual versus the predicted values of the %dye removal are plotted in Figure 16, supporting a good agreement between the observed and predicted values.

3.5 Optimization and Model Validation

To optimize the photodegradation process, target criteria were set to maximize the % pho-

Table 4: ANOVA results of the MB photodegradation model.

Source	Sum of Squares	df	Mean Square	F-Value	p-value Prob > F	
Model	9867.64	14	704.83	84.76	< 0.0001	significant
A-Initial con. (mg/L)	273.47	1	273.47	32.89	< 0.0001	
B-pH	5557.39	1	5557.39	668.33	< 0.0001	
C-Adsorbent dose (mg/L)	1921.86	1	1921.86	231.12	< 0.0001	
D-Time (min)	730.89	1	730.89	87.90	< 0.0001	
AB	490.51	1	490.51	58.99	< 0.0001	
AD	37.98	1	37.98	4.57	0.0495	
BC	719.98	1	719.98	86.58	< 0.0001	
CD	82.40	1	82.40	9.91	0.0066	

todegradation efficiency, with four experimental parameters (*i.e.*, initial dye concentration, solution pH, adsorbent dose, and contact time) chosen in the ranges considered in this study. The optimal solution was based on a desirability value of 1. Under optimal conditions, the best maximum % photodegradation efficiency of 98.60 was found to be at the initial dye concentration of 10.93 mg/L, the solution pH of 8.87, adsorbent dose of 986.43 mg/L, and contact time of 89.08 min (Figure 17). To validate the model's predicted results, additional experiments were conducted at the optimal experimental conditions in three replicates. The average % photodegradation efficiency of these three replicates was found to be 98%, which agrees with the predicted MB removal of 98.60%. It indicates the applicability of using a central composite design (CCD) to optimize and evaluate MB photodegradation by (G-CuO/TiO_2).

3.6 Comparative Study of MB Photodegradation with Other Catalysts

Table 5 shows the photo efficiency (%) of MB by (G-CuO/TiO_2) compared with other catalysts. (G-CuO/TiO_2) is an efficient catalyst for the photodegradation of MB dye.

4. Conclusion

The CuO-TiO_2 was prepared using green extract *Citrus aurantium* juice to obtain (G-CuO/TiO_2) that was used in the degradation of methylene blue under UV lamps and a dark environment. The findings obtained are listed as follows: The photodegradation efficiency of MB by green (G-CuO/TiO_2) was higher than those of (CuO/TiO_2) under visible light irradiation. The current findings suggest that plant-derived nanoparticles could one day be used by industry as a powerful photocatalytic agent to

Table 5. Green synthesized metal oxides of MB dyes degradation.

Reductant	Degradation Conditions	Catalyst	Photo Efficiency, %	Radiation Time, h	Ref.
Citrus Aurantium Juice (CA) extract	10.93 mg/L, 986.43 mg/L, and the solution pH , UV light	TiO_2/CuO/CA	98.6	1.48	This work
Citrus maxima (Pomelo)	5 ppm, 150 mg, pH = 11, UV light	SnO_2	> 90	0.83	[41]
Monsonia burkeana	20 ppm, 20 mg, UV light	ZnO	48	0.8	[42]
Trigonella foenum graecum	25 ppm, pH = 11, UV light	ZnO	88	1.5	[43]
Calotropis praera leaves	20 ppm, 1.5 g/L, UV light	ZnO	81	1.4	[44]
Artocarpus gomezianus	5 ppm, 50 mg, sunlight & UV light, pH = 10	ZnO	90	2.0	[45]
Commelina benghanlensis	20 ppm, 30 mg, UV light, pH = 4	ZnO	81	2.0	[46]
Rueli tuberosa	10 ppm, 20 mg, UV light	Dy_2O_3-SiO_2	94	2.5	[47]

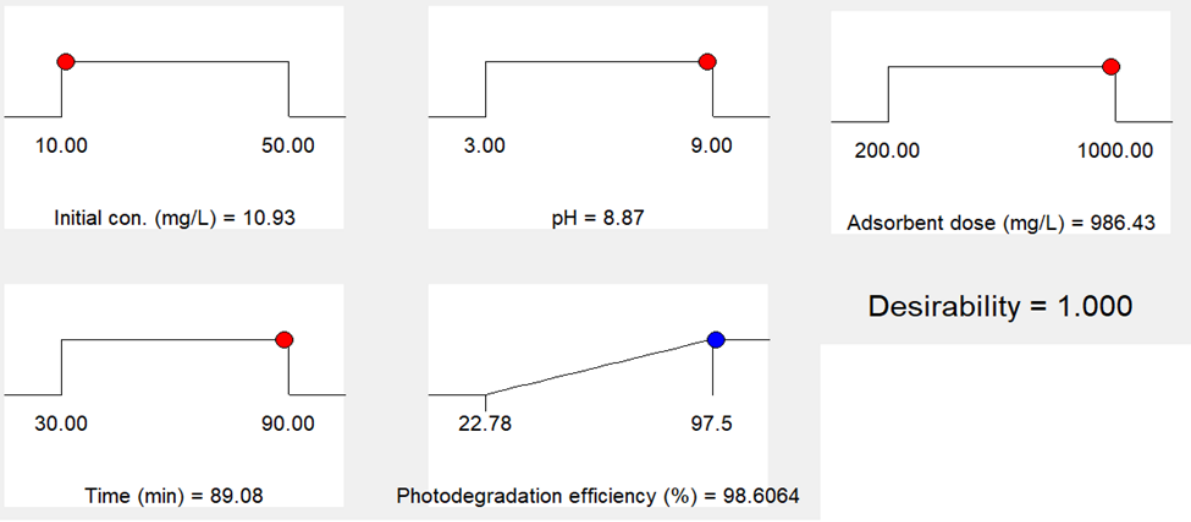

Figure 17. Desirability ramp for the numerical optimization of four selected variables.

clean up contaminated locations. Green technology was employed to produce titanium dioxide particles with biomolecule-loaded copper oxides straightforwardly and affordably. The coprecipitation method was used in this study to create CuO-TiO_2 nanoparticles with (CA) bitter orange juice extract. The most effective photocatalyst for dye oxidation was discovered to be the produced TiO_2 nanoparticles. The current findings suggest that plant-derived nanoparticles could one day be used by industry as a powerful photocatalytic agent to clean up contaminated locations.

Acknowledgment

The authors would like to thank the University of Technology, Baghdad, Iraq for their support in completing this research work.

CRediT Author Statement

Author Contributions: Alyaa K. Mageed, Adnan A. AbdulRazak: Conceptualization, Methodology, Investigation, Resources, Data Curation, Writing, Review and Editing, Supervision; Shahnaz Bassim: Conceptualization, Methodology, Formal Analysis, Data Curation, Writing Draft Preparation, Visualization, Software, Project Administration; Farooq Al-Sheikh: Investigation, Resources, Writing, Review and Editing, Validation. All authors have read and agreed to the published version of the manuscript.

References

[1] Al-Dahri, T., Abdulrazak, A.A., Rohani, S. (2022). Preparation and characterization of Linde-type A zeolite (LTA) from coal fly ash by microwave assisted synthesis method: Its application as adsorbent for removal of anionic dyes. *International Journal of Coal Preparation and Utilization*, 42, 2064–2077. DOI: 10.1080/19392699.2020.1792456.

[2] Ahmed, F.S., Abdulrazak, A.A., Alsaffar, M.A. (2022). Modelling and optimization of methylene blue adsorption from wastewater utilizing magnetic marble dust adsorbent: A response surface methodology approach. *Materials Today: Proceedings*, 60, 1676–1688. DOI: 10.1016/j.matpr.2021.12.224.

[3] Ahmad, M., Rehman, W., Khan, M.M., Qureshi, M.T., Gul, A., Haq, S., Ullah, R., Rab, A., Menaa, F. (2021). Phytogenic fabrication of ZnO and gold decorated ZnO nanoparticles for photocatalytic degradation of Rhodamine B. *Journal of Environmental Chemical Engineering*, 9, 104725. DOI: 10.1016/j.jece.2020.104725.

[4] Abdulrazak, A.A., Shakor, Z.M., Rohani, S. (2018). Optimizing Biebrich Scarlet removal from water by magnetic zeolite 13X utilizing response surface method. *Journal of Environmental Chemical Engineering*, 6, 6175–6183. DOI: 10.1016/j.jece.2018.09.043.

[5] Bassim, S., Mageed, A.K., AbdulRazak, A.A., Majdi, H.S. (2022). Green Synthesis of Fe3O4 Nanoparticles and Its Applications in Wastewater Treatment. *Inorganics*, 10(12), 260. DOI: 10.3390/inorganics10120260.

[6] Ahmed, F.S., Alsaffar, M.A., AbdulRazak, A.A. (2022). One-step synthesis of magnetic fly ash composites for methylene blue removal: batch and column study. *Environmental Science and Pollution Research*, in press. DOI: 10.1007/s11356-022-23491-x.

[7] Majid, Z., Abdulrazak, A.A., Noori, W.A.H. (2019). Modification of zeolite by magnetic nanoparticles for organic dye removal. *Arabian Journal for Science and Engineering*, 44, 5457–5474. DOI: 10.1007/s13369-019-03788-9.

[8] Santoso, E., Ediati, R., Kusumawati, Y., Bahruji, H., Sulistiono, D.O., Prasetyoko, D. (2020). Review on recent advances of carbon-based adsorbent for methylene blue removal from waste water. *Materials Today Chemistry*, 16, 100233. DOI: 10.1016/j.mtchem.2019.100233.

[9] Dzinun, H., Ichikawa, Y., Honda, M., Zhang, Q. (2020). Efficient Immobilised TiO_2 in Polyvinylidene fluoride (PVDF) Membrane for Photocatalytic Degradation of Methylene Blue. *Journal of Membrane Science and Research*, 6, 188–195. DOI: 10.22079/JMSR.2019.106656.1263.

[10] Al-Dhabi, N.A., Arasu, M.V. (2018). Environmentally-friendly green approach for the production of zinc oxide nanoparticles and their anti-fungal, ovicidal. and larvicidal properties. *Nanomaterials*, 8(7), 500. DOI: 10.3390/nano8070500.

[11] Ali, S., Khan, S.A., Khan, I., Yamani, Z.H., Sohail, M., Morsy, M.A. (2017). Surfactant-free synthesis of ellipsoidal and spherical shaped TiO_2 nanoparticles and their comparative photocatalytic studies. *Journal of Environmental Chemical Engineering*, 5, 3956–3962. DOI: 10.1016/j.jece.2017.07.066.

[12] Mohammed, H.A., Khaleefa, S.A., Basheer, M.I. (2021). Photolysis of Methylene Blue Dye Using an Advanced Oxidation Process (Ultraviolet Light and Hydrogen Peroxide). *Journal of Engineering and Sustainable Development*, 25(1), 59–67. DOI: 10.31272/jeasd.25.1.5.

[13] Wang, S.J., Sun, H.P., Qiao, P.Z., Li, Z.Z., Xie, Y., Zhou, W. (2021). NiS/Pt Nanoparticles Co-Decorated Black Mesoporous TiO_2 Hollow Nanotube Assemblies as Efficient Hydrogen Evolution Photocatalysts. *Applied Materials Today*, 22, 100977. DOI: 10.1016/j.apmt.2021.100977.

[14] De Pasquale, I., Lo Porto, C., Dell'Edera, M., Petronella, F., Agostiano, A., Curri, M.L., Comparelli, R. (2020). Photocatalytic TiO2-Based Nanostructured Materials for Microbial Inactivation. *Catalysts*, 10, 1382. DOI: 10.3390/catal10121382.

[15] Gandhi, P.R., Jayaseelan, C., Kamaraj, C., Rajasree, S.R., Mary, R.R. (2018). In vitro antimalarial activity of synthesized TiO2 nanoparticles using Momordica charantia leaf extract against Plasmodium falciparum. *Journal of Applied Biomedicine*, 16(4), 378-386. DOI: 10.1016/j.jab.2018.04.001.

[16] Goutam, S.P., Saxena, G., Singh, V., Yadav, A.K., Bharagava, R.N., Thapa, K.B. (2018). Green synthesis of TiO2 nanoparticles using leaf extract of Jatropha curcas L. for photocatalytic degradation of tannery wastewater. *Chemical Engineering Journal*, 336, 386-396. DOI: 10.1016/j.cej.2017.12.029.

[17] Jegadeeswaran, P., Rajiv, P., Vanathi, P., Rajeshwari, S., Venckatesh, R. (2016). A novel green technology: synthesis and characterization of Ag/TiO2 nanocomposites using Padina tetrastromatica (seaweed) extract. *Materials Letters*, 166, 137-139. DOI: 10.1016/j.matlet.2015.12.058.

[18] Xu, T., Li, C., Li, H., Bai, J., Qin, H., Sun, W., Huang, Y. (2014). Synthesis and Characterization of Cu Nanoparticles Embedded in PAN/ß-Cyclodextrin (ß-CD) Composite Nanofiber Films. *Particulate Science and Technology*, 32(3), 306-310. DOI: 10.1080/02726351.2013.856976.

[19] Raorane, D.V., Chavan, P.S., Pednekar, S.R., Chaughule, R.S. (2017). Green and Rapid Synthesis of Copper-Doped TiO_2 Nanoparticles with Increased Photocatalytic Activity. *Advances in Chemical Science*, 6, 13–20. DOI: 10.14355/sepacs.2017.06.002.

[20] Haider, A., Ali, G., Haider, M.J., Edan, M.S., Al-Obaidy, R., Thamir, A., Hathal, M.M., Abbas, E.M., Al-Sheikh, F. (2022). Modification optical properties of TiO2 nanostructure as solar cell. *Energy Reports*, 8, 77-85. DOI: 10.1016/j.egyr.2022.06.097.

[21] Azzaz, A.A., Assadi, A.A., Jellali, S., Bouzaza, A., Wolbert, D., Rtimi, S., Bousselmi, L. (2018). Discoloration of simulated textile effluent in continuous photoreactor using immobilized titanium dioxide: Effect of zinc and sodium chloride. *Journal of Photochemistry and Photobiology A: Chemistry*, 358, 111–120. DOI: 10.1016/j.jphotochem.2018.01.032.

[22] Daneshvar, N., Rasoulifard, M.H., Khataee, A.R., Hosseinzadeh, F. (2007). Removal of C.I. Acid Orange 7 from aqueous solution by UV irradiation in the presence of ZnO nanopowder. *Journal of Hazardous Materials*, 143, 95–101. DOI: 10.1016/j.jhazmat.2006.08.072.

[23] Zhang, X., Wang, G., Liu, X., Wu, J., Li, M., Gu, J., Li, H., Fang, B. (2008). Different CuO nanostructures: synthesis, characterization, and applications for glucose sensors. *The Journal of Physical Chemistry C*, 112(43), 16845–16849. DOI: 10.1021/jp806985k.

[24] Wang, G., Huang, J., Chen, S., Gao, Y., Cao, D. (2011). Preparation and supercapacitance of CuO nanosheet arrays grown on nickel foam. *Journal of Power Sources*, 196, 5756–5760. DOI: 10.1016/j.jpowsour.2011.02.049.

[25] Munir, S., Shah, S.M., Hussain, H. (2016). Effect of carrier concentration on the optical band gap of TiO2 nanoparticles. *Materials & Design*, 92, 64-72. DOI: 10.1016/j.matdes.2015.12.022.

[26] Daffalla, S.B., Mukhtar, H. Shaharun, M.S. (2010). Characterization of adsorbent developed from rice husk: effect of surface functional group on phenol adsorption. *Journal of Applied Sciences*, 10(12), 1060-1067. DOI: 10.3923/jas.2010.1060.1067.

[27] Khan, A.Q., Yuan, S., Niu, S., Liu, F., Feng, G., Jiang, M., Zeng, H. (2018). Photocatalytic dye degradation with copper–titanium dioxide nanocomposites under sunlight and visible light irradiation, *Materials Research Express*, 5(1), 015030. DOI: 10.1088/2053-1591/aaa361.

[28] Wu, C.Y., Tu, K.J., Deng, J.P., Lo, Y.S., Wu, C.H. (2017). Markedly Enhanced Surface Hydroxyl Groups of TiO_2 Nanoparticles with Superior Water-Dispersibility for Photocatalysis. *Materials*, 10(5), 566. DOI: 10.3390/ma10050566.

[29] Tasbihi, M., Kočí, K., Troppová, I., Edelmannová, M., Reli, M., Čapek, L., Schomäcker, R. (2018). Photocatalytic reduction of carbon dioxide over Cu/TiO_2 photocatalysts. *Environmental Science and Pollution Research*, 25, 34903–34911. DOI: 10.1007/s11356-017-0944-8.

[30] Rahman, M.M., Jamal, A., Khan, S.B., Faisal, M. (2011). Highly sensitive ethanol chemical sensor based on Ni-doped SnO_2 nanostructure materials. *Biosensors and Bioelectronics*, 28(1), 127-134. DOI: 10.1016/j.bios.2011.07.024.

[31] Marimuthu, S., Rahuman, A.A., Jayaseelan, C., Kirthi, A.V., Santhoshkumar, T., Velayutham, K., Bagavan, A., Kamaraj, C., Elango, G., Iyappan, M., Siva, C., Karthik, L., Rao, K.V.B. (2013). Acaricidal activity of synthesized titanium dioxide nanoparticles using Calotropis gigantea against Rhipicephalus microplus and Haemaphysalis bispinosa. *Asian Pacific Journal of Tropical Medicine*, 6(9), 682-688. DOI: 10.1016/S1995-7645(13)60118-2.

[32] Santhoshkumar, T., Rahuman, A.A., Jayaseelan, C., Rajakumar, G., Marimuthu, S., Kirthi, A.V., Thomas, J., Venkatesan, J., Kim, S.K. (2014). Green synthesis of titanium dioxide nanoparticles using Psidium guajava extract and its antibacterial and antioxidant properties. *Asian Pacific Journal of Tropical Medicine*, 7(12), 968-976. DOI: 10.1016/S1995-7645(14)60171-1.

[33] Borhade, A.V., Tope, D.R., Uphade, B.K. (2012). An Efficient Photocatalytic Degradation of Methyl Blue Dye by Using Synthesised PbO Nanoparticles. *Journal of Chemistry*, 9, 362680. DOI: 10.1155/2012/362680.

[34] Pourahmad, A. (2015). Fabrication of nanocatalyst in aqueous solution with photocatalytic activity of methylene blue. *Synthesis and Reactivity in Inorganic, Metal-Organic, and Nano-Metal Chemistry*, 45(7), 1080-1086. DOI: 10.1080/15533174.2013.862656.

[35] Al-Jemeli, M., Mahmoud, M.A., Majdi, H.S., Abid, M.F., Abdullah, H.M., AbdulRazak, A.A. (2021). Degradation of Anti- Inflammatory Drugs in Synthetic Wastewater by Solar Photocatalysis. *Catalysts*, 11, 1330. DOI: 10.3390/catal11111330.

[36] Isai, K.A., Shrivastava, V.S. (2019). Photocatalytic degradation of methylene blue using ZnO and 2%Fe–ZnO semiconductor nanomaterials synthesized by sol–gel method: A comparative study. *SN Applied Sciences*, 1, 1247. DOI: 10.1007/s42452-019-1279-5.

[37] Sahoo, C., Gupta, A.K., Sasidharan Pillai, I.M. (2012). Photocatalytic degradation of methylene blue dye from aqueous solution using silver ion-doped TiO_2 and its application to the degradation of real textile wastewater. *Journal of Environmental Science and Health, Part A*, 47(10), 1428-1438. DOI: 10.1080/10934529.2012.672387.

[38] Saeed, K., Khan, I., Park, S.Y. (2015). TiO_2/amidoxime-modified polyacrylonitrile nanofibers and its application for the photodegradation of methyl blue in aqueous medium. *Desalination and Water Treatment*, 54, 3146–3151. DOI: 10.1080/19443994.2014.912157.

[39] Atarod, M., Nasrollahzadeh, M., Sajadi, S.M. (2016). Euphorbia heterophylla leaf extract mediated green synthesis of Ag/TiO_2 nanocomposite and investigation of its excellent catalytic activity for reduction of variety of dyes in water. *Journal of Colloid and Interface Science*, 462, 272–279. DOI: 10.1016/j.jcis.2015.09.073.

[40] Abdellah, M.H., Nosier, S.A., El-Shazly, A.H., Mubarak, A.A. (2018). Photocatalytic decolorization of methylene blue using TiO_2/UV system enhanced by air sparging. *Alexandria Engineering Journal*, 57(4), 3727-3735. DOI: 10.1016/j.aej.2018.07.018.

[41] Begum, S., Devi, T.B., Ahmaruzzaman, M. (2016). L-lysine monohydrate mediated facile and environment friendly synthesis of SnO_2 nanoparticles and their prospective applications as a catalyst for the reduction and photodegradation of aromatic compounds. *Journal of Environmental Chemical Engineering*, 4, 2976-2989. DOI: 10.1016/j.jece.2016.05.024.

[42] Davar, F., Majedi, A., Mirzaei, A. (2015). Green synthesis of ZnO nanoparticles and its application in the degradation of some dyes. *Journal of the American Ceramic Society*, 98(6), 1739–1746. DOI: 10.1111/jace.13467.

[43] Vinayagam, R., Selvaraj, R., Arivalagan, P., Varadavenkatesan, T. (2020). Synthesis, characterization and photocatalytic dye degradation capability of Calliandra haematocephala-mediated zinc oxide nanoflowers. *Journal of Photochemistry and Photobiology B: Biology*, 203, 111760. DOI: 10.1016/j.jphotobiol.2019.111760.

[44] Prasad, A.R., Garvasis, J., Oruvil, S.K., Joseph, A. (2019). Bio-inspired green synthesis of zinc oxide nanoparticles using Abelmoschus esculentus mucilage and selective degradation of cationic dye pollutants. *Journal of Physics and Chemistry of Solids*, 127, 265–274. DOI: 10.1016/j.jpcs.2019.01.003.

[45] Siripireddy, B., Mandal, B.K. (2017). Facile green synthesis of zinc oxide nanoparticles by Eucalyptus globulus and their photocatalytic and antioxidant activity. *Advanced Powder Technology*, 28, 785–797. DOI: 10.1016/j.apt.2016.11.026.

[46] Rana, N., Chand, S., Gathania, A.K. (2016). Green synthesis of zinc oxide nano-sized spherical particles using Terminalia chebula fruits extract for their photocatalytic applications. *International Nano Letters*, 6, 91–98. DOI: 10.1007/s40089-015-0171-6.

[47] Mahdavi, K., Zinatloo-Ajabshir, S., Yousif, Q.A., Salavati-Niasari, M. (2022). Enhanced photocatalytic degradation of toxic contaminants using Dy_2O_3-SiO_2 ceramic nanostructured materials fabricated by a new, simple and rapid sonochemical approach. *Ultrasonics Sonochemistry*, 82, 105892. DOI: 10.1016/j.ultsonch.2021.105892.